Unraveling Gene–Gene Interactions Regulated by Ligands of the Aryl Hydrocarbon Receptor*

Charles D. Johnson,[1,2] Yoganand Balagurunathan,[3] Mahlet G. Tadesse,[4] M. Hadi Falahatpisheh,[1,2] Marcel Brun,[1,3] Mary K. Walker,[5] Edward R. Dougherty,[3] and Kenneth S. Ramos[1,2]

[1]Department of Biochemistry and Molecular Biology and Center for Genetics and Molecular Medicine, University of Louisville, Louisville, Kentucky, USA; Departments of [2]Veterinary Physiology and Pharmacology, [3]Electrical Engineering, and [4]Statistics, Texas A&M University, College Station, Texas, USA; [5]Department of Pharmacology and Toxicology, University of New Mexico, Albuquerque, New Mexico, USA

The co-expression of genes coupled to additive probabilistic relationships was used to identify gene sets predictive of the complex biological interactions regulated by ligands of the aryl hydrocarbon receptor (*Ahr*). To maximize the number of possible gene–gene combinations, data sets from murine embryonic kidney, fetal heart, and vascular smooth muscle cells challenged *in vitro* with ligands of the *Ahr* were used to create predictor/training data sets. Biologically relevant gene predictor sets were calculated for *Ahr*, cytochrome P450 1B1, insulin-like growth factor–binding protein-5, lysyl oxidase, and osteopontin. Transcript levels were categorized into ternary expressions and target genes selected from the data set and tested for all possible combinations using three gene sets as predictors of transitional level. The goodness of prediction for each set was quantified using a multivariate nonlinear coefficient of determination. Evidence is presented that predictor gene combinations can be effectively used to resolve gene–gene interactions regulated by *Ahr* ligands. *Key words:* aryl hydrocarbon receptor, bioinformatics, gene networks, genomics. *Environ Health Perspect* 112:403–412 (2004). doi:10.1289/txg.6758 available via *http://dx.doi.org/* [Online 14 January 2004]

The assumption that deconstructive methodologies accurately describe the complexity of biological processes is inadequate at best. Until recently, functional genetic studies have been of limited scope and able to elucidate the role of only one or a few genes at a time. Several limitations render these techniques nonconducive to large-scale expression analysis; therefore, nucleotide hybridization technologies are now used to monitor the expression of thousands of genes at a given point in time. A fundamental goal of genomics research is to understand individual gene expression patterns within the symphonic context of the transcriptome and to unravel the genetic networks responsible for health and disease. However, the interactive gene networks responsible for expression of altered cellular phenotypes have not been fully defined.

To date, most microarray experiments have used correlation analysis to identify common genomic responses to a particular stimulus, or multivariate methodologies to examine more complex gene–gene interactions. Univariate methodologies can be used to identify common genomic responses to a particular stimulus but do not account for multiple influences on gene expression. Logistic regression and stepwise regression, on the other hand, are multivariate approaches successfully used to examine more complex genomic interactions but require prior knowledge of the system and assume linearity in assigning biological relatedness.

To understand the complex nature of cellular transformation in cancer, computational prediction methodology has been used to examine global patterns of gene expression (Kim et al. 2000a, 2000b). This method identifies associations between the expression patterns of individual genes by determining whether knowledge of the transcriptional levels of a small gene set predicts the associated transcriptional state of another gene. Although mRNA is not the final product of a gene, transcription is a critical component in the regulatory cascade and therefore provides an ideal point of investigation. A key goal in networks analysis is the development of analytical tools to delineate how individual gene actions are integrated into complex biological systems at the organelle, cell, organ, and organism levels.

The goal of this study was to unravel biological networks regulated by ligands of the aryl hydrocarbon receptor (*Ahr*). *Ahr* is a ligand-activated transcription factor involved in the regulation of cellular growth, differentiation, and metabolism in all species examined (Carlson and Perdew 2002). *Ahr* is a member of the large basic helix–loop–helix–PAS (bHLH-PAS) homology domain family of transcription factors that includes proteins involved in myoblast differentiation, such as myogenic differentiation antigen 1; the cellular response to hypoxia, such as *Ahr* nuclear translocator (*Arnt*) and hypoxia-inducible factor-1; the *Drosophila* neurogenic protein Sim (single-minded), and the *Drosophila* circadian rhythm protein Per (period). bHLH-PAS proteins generally form heterodimeric transcription factors, of which *Ahr* is the only member conditionally activated in response to ligand binding. Polycyclic aromatic hydrocarbon contaminants and by-products of aspartate aminotransferase metabolism are now recognized as ligands of the *Ahr* (Bittinger et al. 2003). After ligand binding within the PAS domain, the cytosolic *Ahr* undergoes a conformational change, dissociates from two 90-kDa heat shock proteins and the hepatitis B virus X-associated protein 2, and translocates to the nucleus where it dimerizes with *Arnt* (Carver and Bradfield 1997). The *Ahr*/*Arnt* heterodimer interacts with *Ahr*-responsive elements (5′-TNGCGTG-3′) upstream of target genes to activate/repress transcription of target genes. Several drug-metabolizing enzymes (Nebert 1994) are regulated by *Ahr*, but key molecular targets involved in regulation of cellular differentiation and growth have remained largely elusive. The complexity of *Ahr* signaling is emphasized by recent studies showing that *Ahr* also participates in post-transcriptional regulation of gene expression (Falahatpisheh and Ramos 2003).

The target genes chosen for study included *Ahr*, cytochrome P450 1B1 (*Cyp1b1*), insulin-like growth factor-binding protein-5 (*Igfbp-5*), lysyl oxidase (*Lox*), and osteopontin (*Opn*). Gene networks were defined on the basis of the co-determination

Address correspondence to K.S. Ramos, Department of Biochemistry and Molecular Biology, University of Louisville Health Sciences Center, Louisville, KY 40292 USA. Telephone: (502) 852-5217. Fax: (502) 852-6222. E-mail: kenneth.ramos@louisville.edu

*The online version of this article (available at http://www.ehponline.org) contains Supplemental Material.

This research was supported by National Institutes of Health grants ES04849, ES09106, ES07273 to K.S.R and ES09804 and ES012072 to M.K.W. C.D.J was supported by National Research Service Award (NSRA) ES012117, M.G.T by National Cancer Institute CA90301, and M.H.F. by NRSA ES012542.

The authors declare they have no competing financial interests.

Received 23 September 2003; accepted 14 January 2004.

of transcriptional states resolved by statistical evaluation of data sets derived from large-scale simultaneous measurements made using Affymetrix microarray technology.

Materials and Methods

Model Systems

Gene transcription information from three independent Affymetrix microarray experiments was used for comprehensive computational analysis. The model systems used included mouse embryonic heart, kidney, and thoracic aorta challenged with hydrocarbon ligands to activate *Ahr* signaling. Vascular smooth muscle cells (vSMC) and fetal kidneys were exposed *in vitro*, whereas fetal hearts were exposed *in vivo*. This approach enabled us to identify common gene sets across tissue types without regard for contextual differences in transcriptional status under basal conditions. The objective was to identify highly conserved interactions regulated by *Ahr* regardless of genomic context.

Data set 1. Vascular smooth muscle cells were isolated from the thoracic aorta of adult C57BL6J untreated mice (Jackson Laboratories, Bar Harbor, ME) (6 weeks of age) and maintained in serial culture as described (Ramos and Cox 1993). All studies were initiated using cells seeded in 150-mm plates at 75% confluence. To induce G_0 synchronization, cultures were incubated for 72 hr in 0.1% fetal bovine serum in Medium 199 (Invitrogen Corp., Carlsbad, CA). Cells were challenged for 8 or 24 hr with dimethyl sulfoxide (DMSO) or 3 µM benzo[*a*]pyrene (B[*a*]P) and RNA was isolated. B[*a*]P is a hydrocarbon ligand of the *Ahr* that modulates growth and differentiation of vascular cells (Kerzee and Ramos 2000). Normalized data from 12 chips were used for the analysis.

Data set 2. Day 11.5 mouse embryos were surgically resected from C57bL/6J wild-type or *Ahr* knockout mice and placed in Hanks' balanced salt solution. Embryonic kidneys (approximately 0.5 mm × 1 mm) were isolated by microsurgical dissection and deposited on culture inserts. B[*a*]P was added to the medium at 3 µM daily for 4 days, and an equivalent volume of DMSO was added to controls. On day 4, kidneys were harvested for RNA isolation. Normalized data from a total of 8 chips were used for analysis.

Data set 3. After exposure to 1.5, 3, and 6 µg/kg 2,3,7,8-tetrachlorodibenzo-*p*-dioxin (TCDD) *in utero* on gestation day 14.5 (n = 4 litters/treatment), gestation day 17.5 fetal mouse hearts were surgically resected and RNA was isolated. TCDD is a potent hydrocarbon ligand that binds and activates *Ahr* signaling. Normalized data from a total of 20 chips were used from this study.

RNA Isolation

Total RNA was extracted using TRI Reagent (Molecular Research Center, Inc., Cincinnati, OH) according to manufacturer's specifications.

Affymetrix GeneChip

The Affymetrix Murine Genome U74A Array (Affymetrix, Inc., Santa Clara, CA) used in these studies represents all functionally characterized sequences (approximately 6,000) in the Mouse UniGene database (http://www.ncbi.nlm.nih.gov/entrez/query.fcgi?db=unigene). In addition, approximately 6,000 expressed sequence tag clusters are included. Experimental procedures including double-stranded cDNA synthesis and biotinylated cRNA preparation were conducted as recommended in the Affymetrix GeneChip Expression Analysis Technical Manual (Affymetrix, Inc. 2003).

Double-Stranded cDNA Synthesis

Total RNA was processed using Qiagen RNeasy kit (Qiagen, Inc., Valencia, CA) according to manufacturer's specifications. For double-stranded cDNA synthesis, 15–20 mg total RNA was first hybridized with 100 pmol T7-(dT)24 primer [5′-(biotin)-GTCGTCAAAGATGCTAC-CGTTCAGCA-3′] and high performance liquid chromatography (GENSET Corp., La Jolla, CA) purified at 70°C for 10 min. Primer hybridization was completed in a 20-mL reaction containing a final concentration of 10 mM dithiothreitol (DTT), 500 mM each of deoxyribonucleoside triphosphate (dNTP) mix, and 1× first-strand cDNA buffer. The reaction was incubated at 42°C for 2 min followed by addition of 400–600 U SuperScript II Reverse Transcriptase (Gibco Life Technologies, Rockville, MD) to synthesize first-strand cDNA. After 1 hr, second-strand cDNA synthesis was carried out by adding 200 mM each dNTP, 10 U *Escherichia coli* DNA ligase, 40 U *E. coli* DNA polymerase I, 20 U *E. coli* RNase H, and 1× second-strand reaction buffer in a 150-mL volume and incubated at 16°C for 2 hr. T4 DNA polymerase was added at the end of the reaction for an additional 5 min and soaked in 10 mL 0.5 M EDTA. Phase Lock Gel (Eppendorf Scientific, Inc., Westbury, NY) extraction with phenol/chloroform followed by ethanol precipitation was subsequently performed to clean up the double-stranded cDNA. The cDNA pellet was resuspended in 12 mL RNase-free water (Ambion, Inc., Austin, TX).

Biotin-Labeled cRNA Preparation

Biotin-labeled cRNA target for hybridization to GeneChip Array (Affymetrix, Inc.) was prepared by *in vitro* transcription using BioArray High Yield RNA Transcript Labeling Kit (Affymetrix, Inc.). Briefly, 3.3–5 mL double-stranded cDNA was mixed gently with 4 mL each of 10× high-yield reaction buffer, 10× biotin-labeled ribonucleotides, 10× DTT, 10× RNase inhibitor mix, and 10× T7 RNA polymerase provided by the kit and incubated at 37°C for 4–5 hr, with gentle mixing every 30 min. Labeled cRNA was then cleaned with RNeasy Mini Kit (Qiagen, Inc.) to obtain an accurate quantification of the labeled cRNA. Twenty to 30 mg labeled cRNA was then fragmented to 35–200 bp with 8 mL 5× fragmentation buffer containing 200 mM Tris-acetate, pH 8.1; 500 mM potassium acetate; and 150 mM magnesium acetate in a total volume of 40 mL for 35 min at 94°C. Before hybridization onto GeneChip Array, the quality of labeling and fragmentation was verified on agarose gel, transferred onto nylon membrane, and detected with alkaline phosphatase streptavidin and DuoLuX Chemiluminescent/Fluorescent Substrate using UltraSNAP Biotinylated Nucleic Acid Detection Kit (Vector Laboratories, Inc., Burlingame, CA).

Hybridization to GeneChip Array

After labeling and fragmentation, 15 µg fragmented biotinylated cRNA was hybridized to the Affymetrix GeneChip Array in a 300-mL cocktail containing 5 mL of 3 nM control oligonucleotide B2, 15 mL 20× eukaryotic hybridization controls, and 150 mL 2× hybridization buffer provided in the GeneChip Eukaryotic Hybridization Control Kit (Affymetrix, Inc.) together with 3 mL 10 mg/mL herring sperm DNA and 3 mL 50 mg/mL acetylated bovine serum albumin (BSA). The hybridization was carried out at 45°C and 60 rpm in GeneChip Hybridization Oven 640 (Affymetrix, Inc.) for 16 hr.

Washing, Staining, and Scanning the Array

After hybridization the washing and staining procedures were carried out on a GeneChip Fluidics Station 400 in conjunction with Affymetrix Microarray Suite 5.0 software (MAS 5.0; Affymetrix, Inc.). Briefly, the array was first washed with 10 cycles of 2 filling and draining cycles in a nonstringent buffer containing 6× SSPE (52.9 g sodium chloride; 8.28 g sodium phosphate; monobasic, 2.82 g EDTA, pH 7.9) and 0.01% Tween 20 at 25°C, followed by 4 cycles of 15 filling and draining cycles in a

stringent buffer containing 100 mM MES [2-(*N*-morpholine)ethanesulfonic acid], 0.1 M Na^+ and 0.01% Tween 20 at 50°C. The probe array then was first stained with a 600-mL streptavidin-phycoerythrin (SAPE) solution containing 1× MES stain buffer (100 mM MES, 1 M Na^+, and 0.05% Tween 20), 2 mg/mL acetylated BSA, and 10 mg/mL SAPE (Molecular Probes, Inc., Eugene, OR) for 10 min at 25°C. After the first staining the array was washed with 10 cycles of 4 filling and draining cycles in nonstringent buffer at 25°C. The stained signals were then amplified in a 600-mL antibody solution containing 1× MES stain buffer, 2 mg/mL acetylated BSA, 0.1 mg/mL normal goat IgG, and 3 mg/mL antistreptavidin biotinylated antibody (Vector Laboratories, Inc.) for 10 min at 25°C, followed by a second SAPE staining at the same temperature for another 10 min. Finally, the probe array was washed for 15 cycles of 4 filling and draining cycles in nonstringent buffer and scanned by the Agilent GeneArray Scanner (Affymetrix, Inc.) at an excitation wavelength of 570 nm.

Data Analysis

After scanning, each image was inspected for major chip defects or abnormalities in hybridization signal as a quality control and analyzed using MAS 5.0. The data were then normalized using a scaling factor of 500 according to the Affymetrix GeneChip Expression Analysis Technical Manual (Affymetrix, Inc. 2003). The expression of approximately 12,000 genes across 40 different Affymetrix microarrays was quantified and normalized. Each of the targets was correlated to the complete Affymetrix gene data set (MATLAB 6.0; The MathWorks, Inc., Natick, MA).

Computational Methodology

After chip normalization, the mean ($\bar{x}$), standard deviation (*sd*) and coefficient of variation

$$cv = sd/\bar{x} \qquad [1]$$

were calculated for each gene across all samples, and the intensity level (x) for each gene was standardized across all arrays by

$$\hat{x} = x - \bar{x}/sd. \qquad [2]$$

All genes were sorted by *cv*, and, because of computational constraints, the 200 clones with the greatest *cv* were selected for use as predictors. The genes to be predicted (i.e., targets) were selected on the basis of biological relevance and included *Ahr*, *Cyp1b1*, *Igfbp-5*, *Lox*, and *Opn*. A heuristic method was used to discretize the data into ternary states that describe their behavior, with –1 used for downregulated genes, 0 for invariant genes, and +1 for upregulated genes. Each array was ordered from lowest to highest standardized values $\hat{x}$ without regard to gene identity and the means across all arrays at the 33rd and 66th percentile were used as the cutoffs for the different values $\bar{x}$ of the standardized data set. These percentiles were chosen because they divided the data evenly to provide sufficient variation throughout the computational analysis. Our goal was to yield good estimates of the transcriptional state of the target using ternary discrete functions. The computation of prediction strengths was completed using a stochastic model of gene intensities, defining X_i as the random variable that represents the ternary intensity (or transcription rate) of gene G_i.

Realizations of X_i were denoted by lower case x_i. A microarray experiment consisted of a realization x_1 to x_v of v random variables X_1 to X_v representing the intensities of the v genes G_1 to G_v. Given N microarrays, the values $x_1(j)$ to $x_v(j)$ represented the values for the microarray j, with $j = 1$ to n. Without loss of generality the predictive strength of genes G_1, G_2, and G_3 over gene G_4 was unknown and therefore needed to be computed. In this context, genes G_1, G_2, and G_3 were regarded as predictors, and G_4 as target. An example of ternary intensity values $x_1(j)$, $x_2(j)$, $x_3(j)$, and $x_4(j)$, $j = 1$ to 9 (or realizations of X_1, X_2, X_3, and X_4), for G_1, G_2, G_3, and G_4, across nine conditions (microarrays) is illustrated in Figure 1 (rows 1–4). The function with the smaller expected error was denoted by ψ_{opt}. The optimal constant function was denoted by ψ_0, and was the one with minimal error over the three possible constant functions.

The optimal functions ψ_{opt} and ψ_0, and their errors $\varepsilon[\psi_{opt}]$ and $\varepsilon[\psi_0]$, respectively, were estimated from the microarray data by splitting them randomly in two sets of conditions, with n conditions for test (estimation of the error) and $N–n$ conditions for train (estimation of the function), where N was the total number of conditions. The optimal function ψ_{opt} and the optimal constant function ψ_0 were estimated from the $N–n$ examples using plug-in rule (Devroye et al. 1996). Let $\hat{\psi}_{opt}$ and $\hat{\psi}_0$ be the estimates of ψ_{opt} and ψ_0, respectively; the errors $\varepsilon[\psi_{opt}]$ and $\varepsilon[\psi_0]$ were estimated using the following equations:

$$\hat{\varepsilon}(\psi_{opt}) = \frac{1}{n}\sum_{j=1}^{n} \left|\hat{\psi}_{opt}(x_1(j), x_2(j), x_3(j)) - x_4(j)\right| \qquad [3]$$

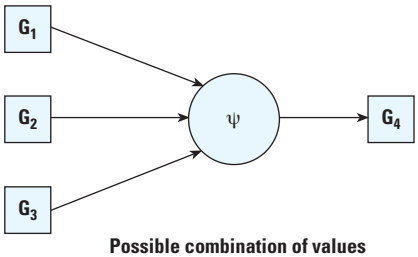

Possible combination of values

	$j=1$	$j=2$	$j=3$	$j=4$	$j=5$	$j=6$	$j=7$	$j=8$	$j=9$
$x_1(j)$	–1	–1	–1	1	0	–1	0	0	0
$x_2(j)$	–1	1	–1	1	0	–1	1	0	–1
$x_3(j)$	–1	0	–1	–1	1	–1	–1	–1	1
$x_4(j)$	–1	0	0	0	0	–1	–1	–1	1
$\psi(x_1,x_2,x_3)$	–1	0	–1	0	1	–1	–1	1	1
$\lvert\psi(x_1,x_2,x_3)–x_4(j)\rvert$	0	0	1	0	1	0	0	2	0
$\psi_0(x_4)$	–1	–1	–1	–1	–1	–1	–1	–1	–1

Figure 1. Schematic representation of gene ternary values and predictor functions ψ. The intensity of genes G_1, G_2, and G_3 can be used to predict the values of the target G_4 via a ternary function ψ. An arbitrary ternary function ψ defined by $\psi(X_1, X_2, X_3) = X_1 + X_2 – X_3$ [with the sum defined inside (–1, 0, 1)] is shown on line 5. The quality of ψ to explain G_4 from G_1, G_2, and G_3 can be measured by its expected absolute error $\varepsilon[\psi] = E[|\psi(X_1, X_2, X_3)–X_4|]$, where | | denotes absolute value, and the expectation is computed over the joint distribution of the random variables X_1, X_2, X_3, and X_4. In line 6, the difference $|\psi(x_1(j), x_2(j), x_3(j)) – x_4(j)|$, for $j = 1$ to 9 is shown to exemplify absolute differences. An estimation of the value of X_4, assuming a constant value, is shown on line 7.

Table 1. Genes that predict selected target gene behavior.[a]

Targets	Predictor	Probe set ID[a]	Percentage[b]	Correlation[c]
Ahr	Lymphocyte antigen 6 complex, locus e	101488_r_at	18	0.77
160495_at	Insulin-like growth factor binding protein 3	95082_at	16	0.83
	Tumor necrosis factor receptor superfamily, member 1b	94928_at	14	0.70
	Insulin-like growth factor binding protein 6	103904_at	13	0.72
	Brain derived neurotrophic factor	102727_at	13	0.80
	Secreted phosphoprotein 1	97519_at	9	0.87
	Stratifin	96704_at	7	0.23
	Small proline-rich protein 2f	94120_s_at	6	0.18
	Actin, alpha, cardiac	101028_i_at	6	–0.84
	NADH dehydrogenase (ubiquinone) 1	100628_at	6	–0.84
	Fibroblast growth factor receptor 4	92937_at	5	0.31
	Ras-related protein	97319_at	5	–0.83
	Small proline-rich protein 2b	99701_f_at	5	0.20
Cyp1b1	Spleen tyrosine kinase	162363_at	31	–0.44
99979_at	Squalene epoxidase	94322_at	18	0.37
	NADH dehydrogenase	92330_r_at	14	0.64
	Calbindin-28k	98133_at	10	–0.20
	Renin 1 structural	98480_s_at	10	–0.10
	Carboxylesterase 3	101539_f_at	10	0.86
	Cytokine receptor-like factor 1	161046_at	9	0.92
	Mitogen regulated protein, proliferin 3	93929_s_at	9	0.92
	Tumor-associated calcium signal transducer 2	160651_at	9	–0.12
	Fos-like antigen 1	99835_at	9	0.89
	Forkhead box a2	93950_at	8	0.86
	Proliferin 2	93883_at	8	0.93
	Thrombomodulin	104601_at	8	0.73
	Fibroblast growth factor 7	99435_at	8	0.94
	Actin, alpha, cardiac	101028_i_at	7	–0.68
	Matrix metalloproteinase 9	99957_at	7	0.13
	Forkhead box f2	99846_at	7	0.70
	Cytochrome p450, 1a1	94715_at	7	0.01
	Insulin-like growth factor 2	98623_g_at	6	–0.03
	Ras-related protein	97319_at	6	–0.65
	Follistatin	98817_at	6	0.73
	Lymphocyte antigen 6 complex, locus A	93078_at	5	0.37
Igfbp-5	Secreted phosphoprotein 1	97519_at	14	–0.64
100566_at	Matrix metalloproteinase 3	98833_at	9	–0.61
	RNA binding motif, single stranded interacting protein 1	96207_at	8	–0.57
	Alpha-2-hs-glycoprotein	99862_at	7	0.27
	Angiotensinogen	101887_at	7	–0.86
	Actin, alpha 1, skeletal muscle	100381_at	7	0.68
	Renin 1 structural	98480_s_at	7	0.23
	Interferon activated gene 202a	94774_at	6	0.04
	Retinol binding protein 4, plasma	96047_at	6	0.40
	Integrin beta 4	103305_at	6	0.43
	Insulin-like growth factor binding protein 3	95082_at	5	–0.40
	Hydroxysteroid 11-beta dehydrogenase 2	100493_at	5	0.24
	Small proline-rich protein 2c	101761_f_at	5	0.09
	Follistatin	98817_at	5	–0.57
	Integrin alpha 6	95511_at	5	0.85
	Carbonic anhydrase 3	160375_at	5	0.26
Lox	Lymphocyte antigen 6 complex, locus H	103487_at	36	–0.37
160095_at	Single stranded interacting protein 1	96207_at	36	0.55
	Glutamyl aminopeptidase	102373_at	23	–0.55
	Peripherin	161482_f_at	21	–0.35
	Cadherin 16	93515_at	16	–0.40
	Coagulation factor II	101899_at	11	–0.30
	Fibroblast growth factor 7	99435_at	11	0.95
	Forkhead box a2	93950_at	11	0.95
	Thrombomodulin	104601_at	11	0.91
	Alcohol dehydrogenase 1, complex	94906_at	9	–0.35
	Fos-like antigen 1	99835_at	9	0.97
	Proliferin 2	93883_at	9	0.93
	Forkhead box f2	99846_at	7	0.87
	Actin, alpha, cardiac	101028_i_at	5	–0.60
	Cyclin-dependent kinase inhibitor 1a (p21)	94881_at	5	–0.53
	High mobility group at-hook 2	99058_at	5	0.85
	Integrin alpha 3	104211_at	5	0.32
	Interferon gamma	99334_at	5	0.53
	Mitogen regulated protein, proliferin 3	93929_s_at	5	0.98
	Phospholipase a2 group VII	101923_at	5	–0.48
	Ras-related	97319_at	5	–0.56

(Continued)

and

$$\hat{\varepsilon}(\psi_0) = \frac{1}{n}\sum_{j=1}^{n} |\hat{\psi}_0(x_1(j), x_2(j), x_3(j)) - x_4(j)|. \quad [4]$$

In our study with $N = 40$, n was defined as $n = N/3$, so $2n$ was used to train the functions and n to estimate the error.

The performance of the predictor set was defined by the coefficient of determination (CoD), that is, the degree to which the transcriptional state of a given set of genes improves the prediction of the transcriptional state of a target gene relative to the best possible constant function (defined by a fixed value) (Devroye et al. 1996) and was defined by

$$\theta = \frac{\varepsilon(\psi_0) - \varepsilon(\psi_{opt})}{\varepsilon(\psi_0)}. \quad [5]$$

The CoD was estimated from the data using the following equation:

$$\theta = \frac{\hat{\varepsilon}(\psi_0) - \hat{\varepsilon}(\psi_{opt})}{\hat{\varepsilon}(\psi_0)}. \quad [6]$$

This process defines an estimate $\hat{\theta}$ of the CoD for the set of predictor genes G_1, G_2, G_3 and the target gene G_4. The process was repeated 1,000 times with different random splitting and the final estimates $\bar{\theta}$ as the average value of $\hat{\theta}$ over the 1,000 replications. The mean error $\bar{\varepsilon}(\psi_{opt})$ was also estimated as the average of the 1,000 estimates $\hat{\varepsilon}(\psi_{opt})$. The higher the CoD, the more accurate the prediction of the target gene transcriptional state derived from the transcriptional state of the three predictor genes. All possible combinations of three predictor genes were studied for each target, where the number of combinations was on the order of 8 million sets of 3 selected from 200, and the estimated CoD $\bar{\theta}$ was computed for all combinations. The predictor sets (or combinations) were ordered from best to worst based on $\bar{\theta}$, and the analysis focused on the predictor combinations with $\bar{\theta} > 0.9$ and $\bar{\varepsilon}(\psi_{opt}) < 0.05$. The cutoff used was selected heuristically to restrict the number of sets to those with good prediction potential. Because of the nature of the analysis, there was no measure of false-positive rates other than future biological experimentation and scrutiny of the literature. Each gene G_i was ranked by f_i, the percentage of sets in this family of good combinations that contain such a gene.

Network Plot

The possible relationships predicted by the predictor algorithm were illustrated using the program developed by Breitkreutz et al. (2003). All three gene combinations that met the cutoff criteria on the basis of test errors and CoD values [$\bar{\theta} > 0.9$ and $\bar{\varepsilon}(\psi_{opt}) < 0.05$] were linked to their respective targets. These schematics were overlaid to form a linkage diagram showing the relationship of target genes to predictors, as well as connections among target genes. The diagrams generated represent the total hypothetical interrelationships between all 200 predictor genes and the five target genes used in the analysis.

Results

The expression of 200 genes across 40 different Affymetrix arrays from three different tissues after activation of *Ahr* signaling was used to predict the behavior of selected targets. *Ahr* activation by a wide range of structurally divergent agents plays a major role in vascular, renal, cardiac, skin, bone marrow, liver, eye, ovary, and immune system function, as well as in carcinogenesis (Denison and Nagy 2003). Table 1 ranks predictor genes by the f_i commonly identified for each target. The *Ahr* receptor itself was most commonly predicted by lymphocyte antigen 6 complex, locus e (selected 18% of the time for all good three-gene combinations), *Igfbp-3* (16%), and tumor necrosis factor receptor super family-member 1b (14%). *Cyp1b1* was best predicted by spleen tyrosine kinase (31%), squalene epoxidase (16%), and nicotinamide adenine dinucleotide (NADH) dehydrogenase (*Ndufc1*) (14%). *Igfbp-5* was most frequently predicted by *Opn* (14%), matrix metalloproteinase 3 (9%), and RNA binding motif–single-stranded interacting protein 1 (8%). *Lox* was best predicted by lymphocyte antigen 6 complex, locus H (*Ly6h*) (36%), single-stranded interacting protein 1 (36%), and glutamyl aminopeptidase (23%). Finally, *Opn* was most often predicted by brain-derived neurotrophic factor (*Bdnf*) (15%), interleukin 6 (14%), and proliferin (14%). The frequency of predictor usage was influenced by the cutoffs used, thus emphasizing the importance of arbitrary cutoff selection. For comparison, each target was also correlated to the complete 12,000 Affymetrix gene data set using normalized intensity values. The results indicated that in many instances genes frequently identified as predictors in the CoD algorithm also exhibited strong correlation to their targets. This is best exemplified for *Ahr* and *Opn*, where *Ndufc1* and α-actin (*Actc1)* exhibited strong correlations and

Table 1. Continued.

Targets	Predictor	Probe set ID[a]	Percentage[b]	Correlation[c]
Opn	Brain derived neurotrophic factor	102727_at	15	0.73
97519_at	Interleukin 6	102218_at	14	0.70
	Proliferin	94838_r_at	14	0.52
	Tumor necrosis factor receptor superfamily, member 1b	94928_at	13	0.76
	Insulin-like growth factor binding protein 3	95082_at	12	0.92
	Gro1 oncogene	95348_at	10	0.73
	Epiregulin	98802_at	9	0.71
	Ras-related protein	97319_at	8	–0.91
	NADH dehydrogenase	100628_at	7	–0.91
	Actin, alpha, cardiac	101028_i_at	7	–0.92
	Actin, alpha 1, skeletal muscle	100381_at	7	–0.85
	Cyclin-dependent kinase inhibitor 1a (p21)	94881_at	6	0.04
	Interferon gamma	99334_at	6	0.38
	Angiopoietin-like 4	96119_s_at	6	0.69
	Cd44 antigen	103005_s_at	5	0.71
	Cytokine receptor-like factor 1	161046_at	5	0.72
	High mobility group at-hook 2	99058_at	5	0.80
	Tumor-associated calcium signal transducer 2	160651_at	5	0.31
	Forkhead box a2	93950_at	5	0.67
	Fos-like antigen 1	99835_at	5	0.72
	Matrix metalloproteinase 3	98833_at	5	0.55

[a]Murine genome U74v2 (for complete details: http://www.affymetrix.com). [b]Percentage representing the number of times a given predictor was used for given target. [c]Linear correlation of the predictor genes to the given target.

were good predictors. As demonstrated by CoD, however, genes exhibiting low correlation to specific targets may play an important role in predicting target behavior. This is exemplified by the best predictor for *Lox*, with a frequency of 36% but a correlation coefficient of only –0.37. Thus, the CoD methodology identified interactions between targets and predictors that could potentially be missed when examined on a gene-by-gene basis.

The complex nature of biological interactions between targets and predictors is illustrated in Figure 2. The linking diagram was built using the f_i ranks for each predictor gene and each target gene. The inclusion of any singular gene does not represent a causal relationship between predictor and target, but rather that gene G_i with two other genes was also a good predictor of a specific target. To some degree, all targets were predictive of each other, a relationship not surprising given that targets were selected *a priori* on the basis of their responsiveness to *Ahr* ligands. Several genes predominated as predictors of each target. These relationships were denoted by the thickness of the connective lines (Figure 2) and the percentage of time used in three gene combinations (Table 1). The number of unique predictors varied with target and cutoff range, with 85% of all possible predictors used to estimate *Ahr*, 63% *Cyp1b1*, 98% *Igfbp-5*, 22% *Lox*, and 53% *Opn*. Given our cutoff range, a total of 34 genes were resolved to provide a comprehensive association of all targets and predictors (Figure 3). The predominant linkages were between all five targets, particularly *Opn* as a predictor of *Ahr* and *Cyp1b1*. The best nontarget predictors included *Bdnf*, *Actc1*, c-*myc* single-strand–binding protein, *Igfbp-6*, and integrin beta4. Figure 4A–E shows the use of individual gene predictor values for construction of three gene predictor set models. It should be noted that predictor genes may lie upstream or downstream from the target or be part of a chain of interaction among various intermediates within the biological network. A large number of three-clone combinations met

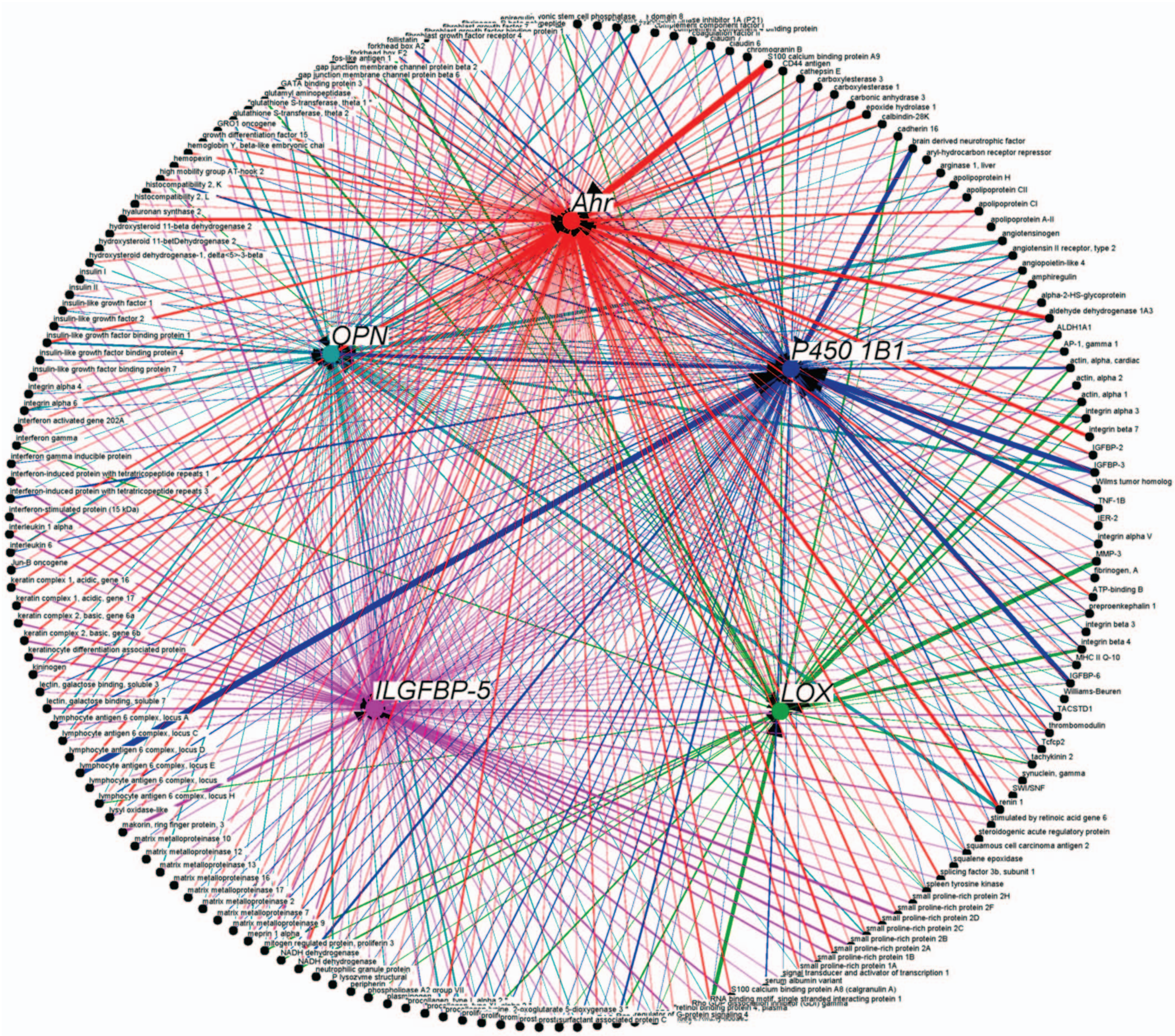

Figure 2. Gene–gene interaction networks activated by ligands of the *Ahr*. All three gene combinations for each target that met the cutoff of COD > 0.9 and error < 0.5 were individually plotted using a program developed by Breitkreutz et al. (2003). The thickness of the line denotes the selection frequency for individual gene for each target.

the selection criteria [($\bar{\theta}$ > 0.9 and $\bar{\varepsilon}(\psi_{opt})$ < 0.05], with one or two clones identified as predominant predictors within the sample pool. A complete listing of target–predictor clone combinations is presented in Table 1 of the Supplemental Material (http://www.ehponline.org).

When examined as three-gene predictor sets, the best combinations for *Ahr* were *Igfbp-3*, lymphocyte antigen 6, and *Actc1* with CoD of 0.963; *Ras*-related, proliferin, and *Igfbp-6* with CoD of 0.96; and thrombomodulin, lymphocyte antigen 6, locus, and *Igfbp-6* with CoD of 0.953 (Figure 4A). The best combinations for *Cyp1b1* were *Ahr*, melanoma growth-simulating activity-alpha (*Gro1*) oncogene, and *Cd44* antigen with CoD of 0.944; *Actc1*, *Bdnf*, and epiregulin with CoD of 0.939; and *Ahr*, *Cd44* antigen, and proliferin 3 with CoD of 0.944 (Figure 4B). The best combinations for *Igfbp-5* were signal transducer and activator of transcription 1 (*Stat1*), *Opn*, and procollagen-lysine, 2-oxoglutarate 5-dioxygenase 3 (*Plod3*) with CoD of 0.98; *Opn*, *Igfbp-1*, and interleukin 1 alpha with CoD of 0.97; and insulin II, *Opn*, and *Igfbp-1* with CoD of 0.97. These combinations performed best when used collectively (Figure 4C). When examined as three gene predictor sets, the best predictor combinations for *Lox* were lymphocyte antigen 6, locus H, *Ndufc1*, and perpherin with CoD of 0.902; perpherin, lymphocyte antigen 6, locus H, and proliferin 2 with CoD of 0.923; and cadherin 16, single-stranded interacting protein 1, and *Cd44* antigen with CoD of 0.924 (Figure 4D). For *Opn* the best three-gene predictor combinations were *Ahr*, *Gro1* oncogene, and *Cd44* antigen with CoD of 0.944; *Actc1*, *Bdnf*, and epiregulin with CoD of 0.939; and *Ahr*, *Cd44* antigen, and proliferin 3 with CoD of 0.944 (Figure 4E).

Discussion

The identification of relevant components of the biological response to *Ahr* ligands was modeled using the transcriptional profiles of cells from murine embryonic heart and kidney or vasculature. Genes whose transcription levels exhibited coupling by CoD methodology were hypothesized to be predictive of one another, whether lying upstream or downstream within the biological network or distributed about the network in such a way that their relation to the target gene was only based on chains of interactions among various intermediate genes. Linear correlation was found to identify predominant genomic responses to a particular stimulus but was unable to identify sets of genes whose actions and interactions drive the transcriptional level of a target. This is problematic, as a gene in and of itself may not be highly correlated to a target but in combination with other genes may be predictive of the behavior of the target. For example, *Ly6h* was identified as the most frequently used *Lox* predictor but showed only modest correlation with *Lox* as a target. Similarly, the small proline-rich proteins 2b and 2f were only poorly correlated to *Ahr* but rank among the top predictors of *Ahr* behavior.

When used individually, each predictor gene exhibited a CoD measure comparable to the value obtained using a linear correlation coefficient model. In contrast the CoD method detected multivariate nonlinear influences on gene expression in complex genetic networks and enabled the calculation of a CoD value that mathematically reflected interactions among all predictors. Use of different treatment modalities was advantageous and allowed identification of genes that move across the transcriptome in unison after activation of *Ahr* signaling regardless of contextual differences in gene expression or tissue-specific patterns of differentiation. For example, the constitutive and inducible expression of *Cyp1b1*, a gene involved in steroidogenesis, is highly tissue specific. *Cyp1b1* is expressed constitutively in the adrenal gland, ovary, and testes and is highly inducible by adrenocorticotropin, cAMP, peptide hormones, and *Ahr* ligands (Buters et al. 2002). *Cyp1b1* is a complex gene, as *Ahr*-independent induction is observed in certain tissues (Kerzee and Ramos 2001), and the gene is overexpressed as a function of transformation (Vondracek et al. 2002). Similarly, *Opn* is differentially expressed under constitutive and inducible conditions and interacts with surface receptors in a context-specific manner. In the normal human kidney, *Cd44* is the primary receptor partner of *Opn*, whereas integrin binding and activation are predominant under stressful conditions (Xie et al. 2001). This dichotomy is also observed within the context of injury, as *Opn* promotes accumulation of macrophages and participates in macrophage-mediated renal injury but exerts renoprotective actions during acute ischemia. Such differences give rise to unique fingerprints that influence gene–gene interactions. Thus, combined data sets within different contextual networks increased the power of the prediction and allowed better integration of biological complexity.

As a biological target, *Ahr* was best predicted by lymphocyte antigen 6e (*Ly6e*), a retinoic acid–responsive gene involved in T-cell activation (Mao et al. 1996; Schedlich

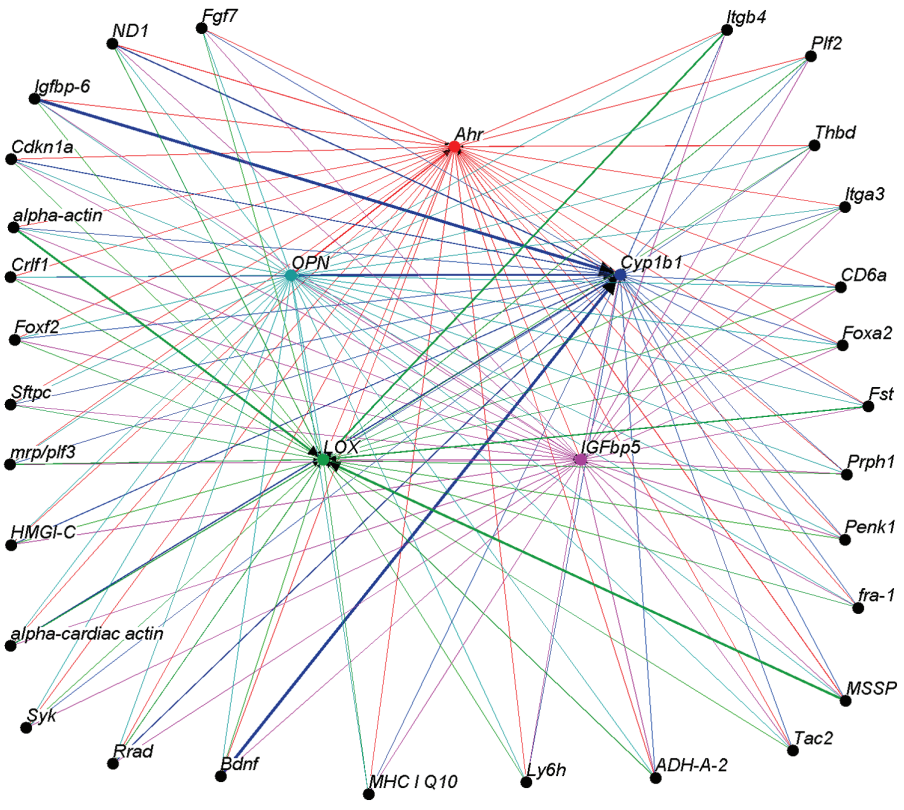

Figure 3. Focused predicted gene networks activated by ligands of the *Ahr*. The common predictor genes across all targets (*Ahr*, *Cyp1b1*, *Igfbp-5*, *Lox*, and *Opn*) are illustrated as described by Breitkreutz et al. (2003) to identify focused gene networks regulated by the *Ahr*.

and Graham 2002). *Ahr* has been implicated in the immune suppressant activity of aromatic hydrocarbons (Kerkvliet et al. 2002) and in the regulation of retinoic acid metabolism. Two other predictor genes for *Ahr*, *Igfbp-3,* and *Igfbp-6*, have also been identified as retinoic acid–regulated genes (Dailly et al. 2001; Schedlich and Graham 2002), suggesting that *Ahr* may couple to predictor genes through retinoic acid linkage (Andreola et al. 1997). Recent studies demonstrate that retinoids activate *Ahr* signaling (Soprano and Soprano 2003), whereas *Ahr* controls the expression of genes involved in retinoic acid metabolism (Gonzalez and Fernandez-Salguero 1998). Thus, computational strategies delineated connections between *Ahr* and retinoic acid that otherwise could not have been predicted in the absence of biological information.

Cyp1b1 was predicted by syk tyrosine kinase (*Syk*) in all cases, a relationship consistent with work by Mounho and Burchiel (1998) showing that oxidative metabolites of B[*a*]P increase tyrosine phosphorylation of *Syk*. *Syk* participates in integrin signaling, leading to nuclear factor-kappa B activation and increased levels of cytokine mRNAs (Lin et al. 1995) and regulation of cancer cell growth and metastasis (Coopman et al. 2000). Similarly, *Ndufc1* appeared in each predictor set, with recent microarray experiments showing common responses in cancer cells for *Cyp1b1* and *Ndufc1* (Huang et al. 2003). *Cyp1b1* catalyzes activation of molecular oxygen in an NADH-dependent electron transport pathway, so a connection with *Ndufc1* and the mitochondrial electron transport chain is consistent with the known biology. Individuals with clefts of the lip and/or palate often share genetic variations in both *Ndufc1* and cytochrome P-450, thus raising intriguing links between the two enzyme systems (Johnston and Bronsky 1995).

In several instances, the algorithm selected a predominant gene, such as *Opn*, when *Igfbp-5* was chosen as a target. *Opn* is a secreted acidic phosphoprotein containing a conserved GRGDS sequence that regulates a variety of cellular processes, primarily through the αvβ3 integrin. *Opn* is a component of the human atherosclerotic plaque that promotes adhesion and spreading of vascular cells and is a potent chemotactic factor for vSMC (Wilson et al. 2002). The strong relationship between *Igfbp-5* and *Opn* is in keeping with studies showing that *Opn* binds to *Igfbp-5* with high affinity (Nam et al. 2000) and that this interaction concentrates *Igfbp-5* on the matrix and modulates cooperative interactions between *Igf-1* receptor and integrin $\alpha_v\beta_3$ in atherosclerotic lesions (Nichols et al. 1999). *Igfbp-5* is the most conserved member of the IGFBP family and a regulator of bone, kidney, and mammary gland function. *Igfbp-5* plays a decisive role in tumor cell proliferation (Schedlich and Graham 2002) and together with *Opn* promotes IGF-I–inducible biological effects. Other genes selected as predictors have been linked to *Igfbp-5*, such as signal transducer and activator of transcription (Chapman et al. 1999) and insulin (Duan et al. 1996).

For other targets, such as *Lox*, the connections between predictor and target gene were less clear. *Lox* is an extracellular and intracellular copper-containing enzyme that initiates cross-linking of collagen and elastin by catalyzing oxidative deamination of the epsilon-amino group in certain

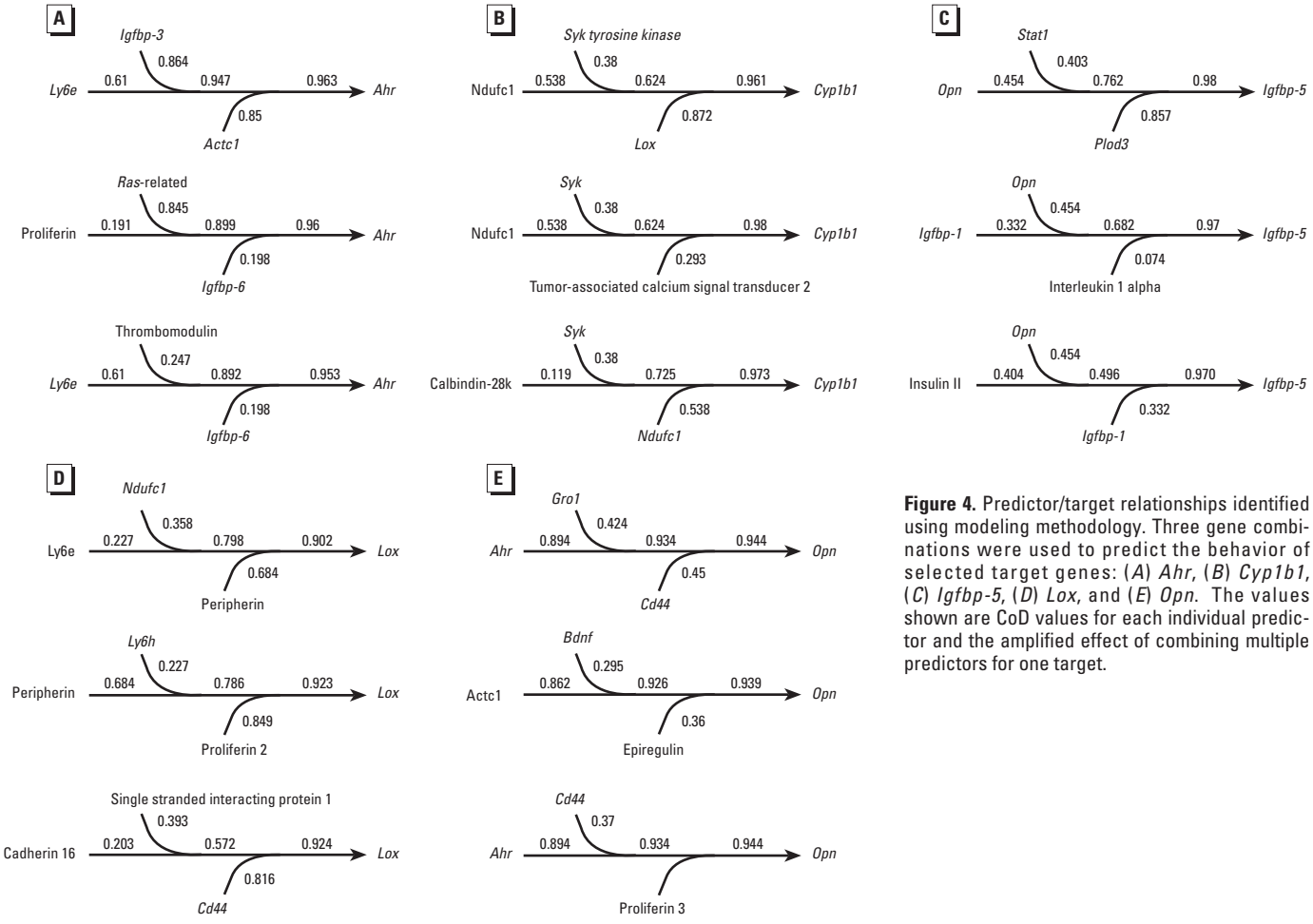

Figure 4. Predictor/target relationships identified using modeling methodology. Three gene combinations were used to predict the behavior of selected target genes: (*A*) *Ahr*, (*B*) *Cyp1b1*, (*C*) *Igfbp-5*, (*D*) *Lox*, and (*E*) *Opn*. The values shown are CoD values for each individual predictor and the amplified effect of combining multiple predictors for one target.

lysine and hydroxylysine residues of collagens and lysine residues of elastin. *Lox* is found in smooth muscle cell nuclei and is speculated to be involved in oxidative deamination of peptidyl lysine (Kuivaniemi et al. 1984; Li et al. 1997). As such, the finding that matrix-related genes such as peripherin and proliferin2 were selected as predictors is of interest. Integrins may link *Lox* and peripherin, with both collagen and peripherin modulated by the $\alpha 2\beta 1$ integrin (Khalsa et al. 2000). The connection with immune-related genes such as *Cd44* and *Ly6h* is intriguing and may involve interferon. Interferon-gamma, a proinflammatory cytokine, downregulates *Lox* gene expression in rat aortic smooth muscle cells (Song et al. 2000), and *Ly6h* has also been identified as a target of interferon (Horie et al.1998). *Lox* and *Ndufc1* are coregulated under sheer stress (Ando et al. 1996), so a link between these two genes may also exist.

The relationship between *Opn* and *Ahr* is intriguing. Recent studies have shown that resveratrol (3,5,4′-trihydroxystilbene), an *Ahr* antagonist, modifies the inhibitory effect of TCDD on *Opn* expression (Singh et al. 2000). *Opn* is a ligand for the *Cd44* receptor and stimulates *Cd44* expression on the osteoclast surface (Chellaiah et al. 2003; Sodek et al. 2002). The relationship between *Cd44* and *Opn* is well established (Denhardt et al. 2001). The analysis also predicted a relationship between *Opn* and *Actc1*, a connection consistent with reports by Shu and co-workers (2002) showing that *Opn*-expressing tubuli in kidney were tightly associated with a peritubular influx of alpha-smooth muscle actin. It is also not surprising that *Opn* expression was predicted by two growth factors such as epiregulin and *Bdnf* (Lee et al. 2001; Toyoda et al. 1995). The observed associations indicate that measurement of the transcriptional state of multiple gene sets can be combined to better predict the expression level of a target gene The strongest interaction between targets was the interplay between *Ahr*, *Cyp1b1*, and *Opn* (Figures 2 and 3). Although these biological connections are novel, they are in keeping with studies showing that *Ahr* signaling is critical to *Opn* regulation (Singh et al. 2000) and that ligands of the *Ahr* modulate *Opn* expression. For some of the target/predictor relationships, no direct linkages could be established. An example is *Bdnf*, a protein that allows the survival of specific neuronal populations and found to be highly predictive of *Opn*. As both *Bdnf* and *Opn* are involved in matrix regulation, the relationship could be an interesting area for future investigation.

Conclusions

Novel putative interactions were defined to investigate gene–gene interactions regulated by the *Ahr*. In many instances, the relevance of the biological relationships uncovered using CoD methodology was ratified by published reports, whereas in others, novel interactions were identified. The computational approach used afforded us the ability to begin constructing gene networks that define broad-ranging interactive biological relationships. Although the biological bases for these theoretical relationships must be investigated further, the number of possible combinations is now reduced to a manageable size that can be systematically scrutinized using established molecular methodologies.

References

Affymetrix, Inc. 2003. GeneChip Expression Analysis Technical Manual, Rev. 4. Santa Clara, CA:Affymetrix, Inc.

Ando J, Tsuboi H, Korenaga R, Takahashi K, Kosaki K, Isshiki M, et al. 1996. Differential display and cloning of shear stress-responsive messenger RNAs in human endothelial cells. Biochem Biophys Res Commun 225:347–351.

Andreola F, Fernandez-Salguero PM, Chiantore MV, Petkovich MP, Gonzalez FJ, De Luca LM. 1997. Aryl hydrocarbon receptor knockout mice (AHR–/–) exhibit liver retinoid accumulation and reduced retinoic acid metabolism. Cancer Res 57:2835–2838.

Bittinger MA, Nguyen LP, Bradfield CA. 2003. Aspartate aminotransferase generates proagonists of the aryl hydrocarbon receptor. Mol Pharmacol 64:550–556.

Breitkreutz BJ, Stark C, Tyers M. 2003. Osprey: a network visualization system. Genome Biol 4:R22.1–R22.4

Buters JT, Mahadevan B, Quintanilla-Martinez L, Gonzalez FJ, Greim H, Baird WM, et al. 2002. Cytochrome P450 1B1 determines susceptibility to dibenzo[*a,l*]pyrene-induced tumor formation. Chem Res Toxicol 15:1127–1135.

Carlson DB, Perdew GH. 2002. A dynamic role for the Ah receptor in cell signaling? Insights from a diverse group of Ah receptor interacting proteins. J Biochem Mol Toxicol 16:317–325.

Carver LA, Bradfield, CA. 1997. Ligand-dependent interaction of the aryl hydrocarbon receptor with a novel immunophilin homolog *in vivo*. J Biol Chem 272:11452–11456.

Chapman RS, Lourenco PC, Tonner E, Flint DJ, Selbert S, Takeda K, et al. 1999. Suppression of epithelial apoptosis and delayed mammary gland involution in mice with a conditional knockout of Stat3. Genes Dev 13:2604–2616.

Chellaiah MA, Kizer N, Biswas R, Alvarez U, Strauss-Schoenberger J, Rifas L, et al. 2003. Osteopontin deficiency produces osteoclast dysfunction due to reduced *Cd44* surface expression. Mol Biol Cell 14:173–189.

Coopman PJ, Do MT, Barth M, Bowden ET, Hayes AJ, Basyuk E, et al. 2000. The Syk tyrosine kinase suppresses malignant growth of human breast cancer cells. Nature 406:742–747.

Dailly YP, Zhou Y, Linkhart TA, Baylink DJ, Strong DD. 2001. Structure and characterization of the human insulin-like growth factor binding protein (*Igfbp*)-6 promoter: identification of a functional retinoid response element. Biochim Biophys Acta 1518:145–151.

Denhardt DT, Giachelli CM, Rittling SR. 2001. Role of osteopontin in cellular signaling and toxicant injury. Annu Rev Pharmacol Toxicol 41:723–749.

Denison MS, Nagy SR. 2003. Activation of the aryl hydrocarbon receptor by structurally diverse exogenous and endogenous chemicals. Annu Rev Pharmacol Toxicol 43:309–334.

Devroye L, Gyorffy L, Lugosi G. 1996. A Probabilistic Theory of Pattern Recognition. New York: Springer-Verlag.

Duan C, Hawes SB, Prevette T, Clemmons DR. 1996. Insulin-like growth factor-I (IGF-I) regulates IGF-binding protein-5 synthesis through transcriptional activation of the gene in aortic smooth muscle cells. J Biol Chem 271:4280–4288.

Falahatpisheh MH, Ramos KS. 2003. Ligand-activated *Ahr* signaling leads to disruption of nephrogenesis and altered Wilms' tumor suppressor mRNA splicing. Oncogene 10:2160–2171.

Gonzalez FJ, Fernandez-Salguero P. 1998. The aryl hydrocarbon receptor: studies using the AHR-null mice. Drug Metab Dispos 26:1194–1198.

Horie M, Okutomi K, Taniguchi Y, Ohbuchi Y, Suzuki M, Takahashi E. 1998. Isolation and characterization of a new member of the human Ly6 gene family (*Ly6h*). Genomics 53:365–368.

Huang E, Ishida S, Pittman J, Dressman H, Bild A, Kloos M, et al. 2003. Gene expression phenotypic models that predict the activity of oncogenic pathways. Nat Genet 34:226–230.

Johnston MC, Bronsky PT. 1995. Prenatal craniofacial development: new insights on normal and abnormal mechanisms. Crit Rev Oral Biol Med 6:368–422.

Kerkvliet NI, Shepherd DM, Baecher-Steppan L. 2002. T lymphocytes are direct, aryl hydrocarbon receptor (AhR)-dependent targets of 2,3,7,8-tetrachlorodibenzo-*p*-dioxin (TCDD): AhR expression in both $CD4^+$ and $CD8^+$ T cells is necessary for full suppression of a cytotoxic T lymphocyte response by TCDD. Toxicol Appl Pharmacol 185:146–152.

Kerzee JK, Ramos KS. 2000. Activation of c-Ha-*ras* by benzo(*a*)pyrene in vascular smooth muscle cells involves redox stress and aryl hydrocarbon receptor. Mol Pharmacol 58:152–158.

———. 2001. Constitutive and inducible expression of *Cyp1a1* and *Cyp1b1* in vascular smooth muscle cells: role of the *Ahr* bHLH/PAS transcription factor. Circ Res 89:573–582.

Khalsa PS, Zhang C, Sommerfeldt D, Hadjiargyrou M. 2000. Expression of integrin $\alpha 2\beta 1$ in axons and receptive endings of neurons in rat, hairy skin. Neurosci Lett 293:13–26.

Kim S, Dougherty ER, Bittner ML, Chen Y, Sivakumar K, Meltzer PS, et al. 2000a. Multivariate measurement of gene expression relationships. Genomics 67:201–209.

———. 2000b. General nonlinear framework for the analysis of gene interaction via multivariate expression arrays. J Biomed Optics 5:411–424.

Kuivaniemi H, Savolainen ER, Kivirikko KI. 1984. Human placental lysyl oxidase: purification, partial characterization, and preparation of two specific antisera to the enzyme. J Biol Chem 259:6996–7002.

Lee R, Kermani P, Teng KK, Hempstead BL. 2001. Regulation of cell survival by secreted proneurotrophins. Science 294:1945–1948.

Li W, Nellaiappan K, Strassmaier T, Graham L,

Thomas KM, Kagan HM. 1997. Localization and activity of lysyl oxidase within nuclei of fibrogenic cells. Proc Nat Acad Sci USA 94:12817–12822.

Lin TH, Rosales C, Mondal K, Bolen JB, Haskill S, Juliano RL. 1995. Integrin-mediated tyrosine phosphorylation and cytokine message induction in monocytic cells. A possible signaling role for the Syk tyrosine kinase. J Biol Chem 270:16189–16197.

Mao M, Yu M, Tong J-H, Ye J, Zhu J, Huang Q-H, et al. 1996. RIG-E, a human homolog of the murine Ly-6 family, is induced by retinoic acid during the differentiation of acute promyelocytic leukemia cell. Proc Nat Acad Sci USA 93:5910–5914.

Mounho BJ, Burchiel SW. 1998. Alterations in human B cell calcium homeostasis by polycyclic aromatic hydrocarbons: possible associations with cytochrome P450 metabolism and increased protein tyrosine phosphorylation. Toxicol Appl Pharmacol 149:80–89.

Nam TJ, Busby WH Jr, Rees C, Clemmons DR. 2000. Thrombospondin and osteopontin bind to insulin-like growth factor (IGF)-binding protein-5 leading to an alteration in IGF-I-stimulated cell growth. Endocrinology 141:1100–1106.

Nebert DW. 1994. Drug metabolism and signal transduction: possible role of Ah receptor and arachidonic acid cascade in protection from ethanol toxicity. EXS 71:231–240.

Nichols TC, du Laney T, Zheng B, Bellinger DA, Nickols GA, Engleman W, et al. 1999. Reduction in atherosclerotic lesion size in pigs by alphaVbeta3 inhibitors is associated with inhibition of insulin-like growth factor-I-mediated signaling. Circ Res 85:1040–1045.

Ramos KS, Cox LR. 1993. Aortic endothelial and smooth muscle cell cultures. Vol 1 (Tyson CA, Frazier JM, eds). In: Methods in Toxicology: In Vitro Biological Systems. St. Louis, MO:Academic Press, 159–168.

Schedlich LJ, Graham LD. 2002. Role of insulin-like growth factor binding protein-3 in breast cancer cell growth. Microsc Res Tech 59:12–22.

Shu Y, Hoshi S, Tomari S, Watanabe T, Nagata M. 2002. Phenotypic changes and cell cycle activation in early tubulointerstitial injury of rat adriamycin nephrosis. Pathol Int 52:214–223.

Singh SU, Casper RF, Fritz PC, Sukhu B, Ganss B, Girard B Jr, et al. 2000. Inhibition of dioxin effects on bone formation *in vitro* by a newly described aryl hydrocarbon receptor antagonist, resveratrol. J Endocrinol 167:183–195.

Sodek J, Zhu B, Huynh MH, Brown TJ, Ringuette M. 2002. Novel functions of the matricellular proteins osteopontin and osteonectin/SPARC. Connect Tissue Res 43:308–319.

Song YL, Ford JW, Gordon D, Shanley CJ. 2000. Regulation of lysyl oxidase by interferon-gamma in rat aortic smooth muscle cells. Arterioscler Thromb Vasc Biol 20:982–988.

Soprano DR, Soprano KJ. 2003. Pharmacological doses of some synthetic retinoids can modulate both the aryl hydrocarbon receptor and retinoid receptor pathways. J Nutr 133:277S–281S.

Toyoda H, Komurasaki T, Uchida D, Takayama Y, Isobe T, Okuyama T, et al. 1995. Epiregulin: a novel epidermal growth factor with mitogenic activity for rat primary hepatocytes. J Biol Chem 270:7495–7500.

Vondracek M, Weaver DA, Sarang Z, Hedberg JJ, Willey JC, Warngard L, et al. 2002. Transcript profiling of enzymes involved in detoxification of xenobiotics and reactive oxygen in human normal and simian virus 40 T antigen-immortalized oral keratinocytes. Int J Cancer 99:776–782.

Wilson E, Parrish AR, Bral CM, Williams ES, Ramos KS. 2002. Collagen suppresses the proliferative phenotype of allylamine-injured vascular smooth muscle cells. Atherosclerosis 162:289–297.

Xie Y, Sakatsume M, Nishi S, Narita I, Arakawa M, Gejyo F. 2001. Expression, roles, receptors, and regulation of osteopontin in the kidney. Kidney Int 60:1645–1657.